

THE ECCENTRIC KOZAI MECHANISM FOR A TEST PARTICLE

YORAM LITHWICK¹ AND SMADAR NAOZ¹

Draft version June 20, 2011

ABSTRACT

We study the dynamical evolution of a test particle that orbits a star in the presence of an exterior massive planet, considering octupole-order secular interactions. In the standard Kozai mechanism (SKM), the planet’s orbit is circular, and so the particle conserves vertical angular momentum. As a result, the particle’s orbit oscillates periodically, exchanging eccentricity for inclination. However, when the planet’s orbit is eccentric, the particle’s vertical angular momentum varies and its Kozai oscillations are modulated on longer timescales—we call this the eccentric Kozai mechanism (EKM). The EKM can lead to behavior that is dramatically different from the SKM. In particular, the particle’s orbit can flip from prograde to retrograde and back again, and it can reach arbitrarily high eccentricities given enough time. We map out the conditions under which this dramatic behavior (flipping and extreme eccentricities) occurs, and show that when the planet’s eccentricity is sufficiently high, it occurs quite generically. For example, when the planet’s eccentricity exceeds a few percent of the ratio of semi-major axes (outer to inner), around half of randomly oriented test particle orbits will flip and reach extreme eccentricities. The SKM has often been invoked for bringing pairs of astronomical bodies (star-star, planet-star, compact-object pairs) close together. Including the effect of the EKM will enhance the rate at which such matchmaking occurs.

1. INTRODUCTION

Naoz et al. (2011a) recently showed that in a system with two planets orbiting a star, the inner planet’s orbit can flip from prograde to retrograde and back, and can also reach extremely high eccentricities. Therefore, starting from a system with two prograde planets on distant orbits from their star, the inner planet can both flip its orbital orientation and reach high enough eccentricities to be tidally captured by the star. That might explain the origin of the $\sim 25\%$ of hot Jupiters whose orbits are retrograde with respect to the spin of their star, as inferred from Rossiter-McLaughlin measurements (e.g., Triaud et al. 2010). However, while the behavior displayed in Naoz et al. (2011a) is intriguing, it has not yet been understood. Furthermore, Naoz et al. (2011a) choose initial eccentricities and inclinations that are fairly extreme for planetary systems ($e \sim 0.6, i \sim 70^\circ$), and hence it is not yet clear how generic their results are. The goal of this paper is to understand and map out the mechanism in a simplified system where the inner planet is treated as a massless test particle.

There has been much work in the literature on the orbital dynamics of similar systems. Kozai (1962) considered the evolution of an asteroid perturbed by a circular Jupiter. He focused on secular interactions, meaning that interactions are averaged over the orbital phases of the asteroid and Jupiter. Kozai found a remarkable result: if the asteroid’s orbit is sufficiently inclined (between 39° and 141°), then it cannot remain on a circular orbit. Instead, its eccentricity and inclination oscillate periodically. Furthermore, if the asteroid is highly inclined ($\sim 90^\circ$), then its eccentricity will grow over the course of a single Kozai oscillation to ~ 1 .

The Kozai mechanism has been applied to a variety of

astronomical systems. For example, in triple star systems, if the outer star is inclined it can force Kozai oscillations in the inner binary, increasing the inner binary’s eccentricity until tidal dissipation circularizes it into a very tight orbit (e.g., Eggleton & Kiseleva-Eggleton 2001; Fabrycky & Tremaine 2007). Similarly, if a Jupiter-mass planet forms around a star with an inclined companion star, that companion can force Kozai oscillations in the planet until tides damp its orbit, forming it into a hot Jupiter (Wu & Murray 2003; Fabrycky & Tremaine 2007). Analogous scenarios have been proposed for merging supermassive black holes (Blaes et al. 2002) and stellar-mass compact objects (Thompson 2010). See also Naoz et al. (2011b) for a review of other applications of the Kozai mechanism.

In the case considered by Kozai, the asteroid’s vertical angular momentum ($=\text{const} \times \sqrt{1-e^2} \cos i$) is conserved because Jupiter’s orbit is circular. Since this is a two degree of freedom system (eccentricity and inclination) with two conserved quantities (vertical angular momentum and secular energy), it is integrable. But when Jupiter’s orbit is eccentric, the dynamics can no longer be solved analytically. As Kozai noted, “[w]ithout the aid of a high-speed computer, it is rather difficult to estimate the effects of Jupiter’s eccentricity.”

The effect of an eccentric perturber on Kozai oscillations has been considered in a number of example cases. Harrington (1969) integrates the secular octupole equations for four triple star systems, and shows that in one case there is a new resonance; in a second case there is chaos; and in the other two cases no new interesting effects arise. Holman et al. (1997) perform a direct numerical integration for a planet forced by a star, but with their parameters ($\epsilon \simeq 0.008$ in our notation, see below), the perturber’s finite eccentricity only leads to a narrow zone of chaos around the Kozai separatrix. Ford et al. (2000) integrate the secular octupole equations for a sys-

¹ Department of Physics and Astronomy, Northwestern University, 2145 Sheridan Rd., Evanston, IL 60208

tem of two eccentric planets, where the outer planet has eccentricity = 0.9, and find that the inner planet’s Kozai oscillations are modulated on long timescales, leading to extreme eccentricities. Blaes et al. (2002) examine some examples for triples of supermassive black holes. Naoz et al. (2011a,b) examine some examples for two planets. Yet a systematic exploration of the effect of an eccentric Kozai perturber is lacking.

In a number of studies the effect of an eccentric perturber on Kozai oscillations has been neglected, even in situations where it should not be (Naoz et al. 2011b). Part of the reason is that treatments of Kozai oscillations often expand the secular Hamiltonian to leading order in the ratio of semimajor axes, i.e. to quadrupole order. At that order, the exterior body’s argument of periaapse does not appear, which implies that the particle’s vertical angular momentum is conserved.² To see the effect of the eccentricity, one must work to higher order in the ratio of semimajor axes, i.e. at least to octupole order.

In this paper, we extend Kozai’s work to the case of an eccentric planet and map out the resulting behavior, which we call the eccentric Kozai mechanism (EKM). To do so, we use the secular octupole Hamiltonian of Ford et al. (2000), which was apparently first derived by Harrington (1968) (as cited by Harrington 1969; see also Marchal 1990 and Krymowski & Mazeh 1999 for derivations).

After the work described here was completed, we learnt of a similar paper being prepared by Katz, Dong, and Malhotra.

This paper is organized as follows. In Section 2, we present the equations of motion, relegating their derivation to the Appendix. In Section 3, we review the SKM. In Section 4, the heart of this paper, we map out the EKM. We summarize in Section 5.

2. EQUATIONS OF MOTION

We solve for the orbit of a massless test particle in the presence of an exterior massive planet, including only secular interactions expanded to octupole order. The planet is on a fixed eccentric orbit, and the particle’s orbit is specified by four variables,

$$\{e, \omega, \theta \equiv \cos i, \Omega\}, \quad (1)$$

which are its eccentricity, argument of periaapse, inclination (or its cosine), and longitude of ascending node relative to the planet’s periaapse (e.g., Murray & Dermott 2000). In the Appendix, we use the secular octupole Hamiltonian that has been published in the literature to derive the particle’s equations of motion. As we show in the Appendix, although that published Hamiltonian has had its nodes eliminated, one can still use it to derive the full test particle equations of motion—even the equation that requires the nodes.

We summarize the equations here. Defining the particle’s (scaled) total angular momentum and vertical an-

gular momentum as³

$$J \equiv \sqrt{1 - e^2} \quad (2)$$

$$J_z \equiv \theta \sqrt{1 - e^2}, \quad (3)$$

the equations of motion may be expressed as partial derivatives of an energy function $F(e, \omega, \theta, \Omega)$ via

$$\frac{dJ}{dt} = \frac{\partial F}{\partial \omega} \quad (4)$$

$$\frac{dJ_z}{dt} = \frac{\partial F}{\partial \Omega} \quad (5)$$

$$\frac{d\omega}{dt} = \frac{\partial F}{\partial e} \frac{J}{e} + \frac{\partial F}{\partial \theta} \frac{\theta}{J} \quad (6)$$

$$\frac{d\Omega}{dt} = -\frac{\partial F}{\partial \theta} \frac{1}{J} \quad (7)$$

where t is proportional to time (Eq. [A8]). These are Hamilton’s equations for the two pairs of canonically conjugate variables $\{J, \omega\}$ and $\{J_z, \Omega\}$, except that we express F as a function of the non-canonical variables e and θ —for that reason, we call F the energy function rather than the Hamiltonian. Of course, F is a constant of the motion. It is given by a quadrupole and an octupole term

$$F \equiv F_{\text{qu}} + \epsilon F_{\text{oc}}, \quad (8)$$

where the constant

$$\epsilon \equiv \frac{(a/a_{\text{pl}})e_{\text{pl}}}{1 - e_{\text{pl}}^2}; \quad (9)$$

here a/a_{pl} is the ratio of semimajor axes (inner to outer) and e_{pl} is the planet’s eccentricity. The quadrupole piece is

$$F_{\text{qu}} \equiv -\frac{e^2}{2} + \theta^2 + \frac{3}{2}e^2\theta^2 + \frac{5}{2}e^2(1 - \theta^2)\cos(2\omega), \quad (10)$$

after dropping an irrelevant constant, and the octupole term is

$$\begin{aligned} F_{\text{oc}} \equiv \frac{5}{16}(e + \frac{3}{4}e^3) & \left[(1 + 11\theta - 5\theta^2 - 15\theta^3)\cos(\omega + \Omega) \right. \\ & \left. + (1 - 11\theta - 5\theta^2 + 15\theta^3)\cos(\omega - \Omega) \right] \\ & - \frac{175}{64}e^3 \left[(1 - \theta - \theta^2 + \theta^3)\cos(3\omega - \Omega) \right. \\ & \left. + (1 + \theta - \theta^2 - \theta^3)\cos(3\omega + \Omega) \right] \quad (11) \end{aligned}$$

The only adjustable parameter in the equations of motion other than the initial conditions is the constant ϵ . That constant encodes the properties of the planet.⁴ In the standard Kozai mechanism (SKM), the planet’s orbit is circular ($\epsilon = 0$). Hence F is independent of Ω , and thus J_z is a constant of the motion. But if the planet’s eccentricity is not zero ($\epsilon > 0$), then the octupole term allows J_z to change. If the planet is either nearly circular ($e_{\text{pl}} \ll 1$) or distant ($a/a_{\text{pl}} \ll 1$), then ϵ is very small,

² The fact that the exterior body’s argument of periaapse does not appear to quadrupole order has been called “a happy coincidence” because it makes the system integrable (Lidov & Ziglin 1976; Laskar & Boué 2010). However, it is perhaps more of an unhappy coincidence in view of the fact that it has misled some researchers into neglecting the role of the planet’s eccentricity.

³ Our variables are related to the Delaunay variables $\{G, g, H, h\}$ that are often used in treatments of Kozai oscillations via $J = G/(m\sqrt{G_N M_* a})$, $\omega = g$, $J_z = H/(m\sqrt{G_N M_* a})$, $\Omega = h$ (Eqs. [A3]–[A4]).

⁴ The planet’s properties also enter in a trivial way through the scaling between t and time (Eq. [A8]).

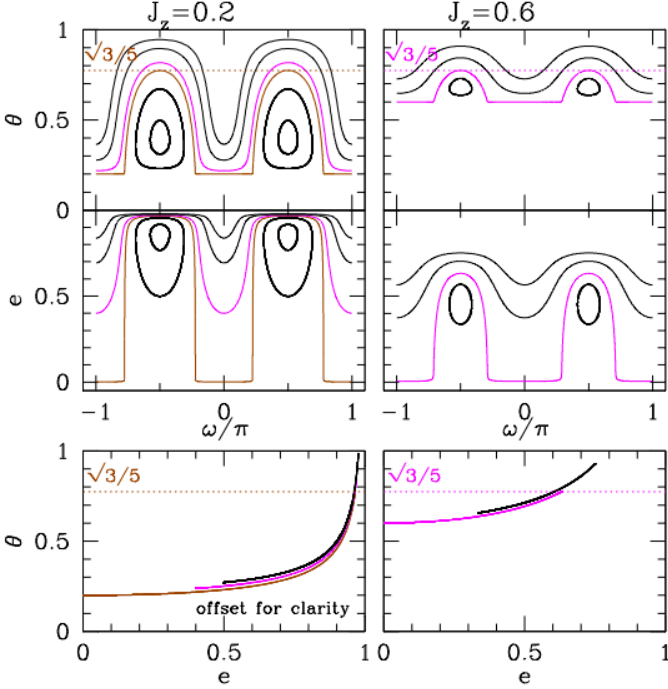


FIG. 1.— SKM ($\epsilon = 0$): The three left panels show trajectories with $J_z = 0.2$ and various values of F . Trajectories with the same J_z overlap in the e - θ plane (bottom panel); we have slightly offset these for clarity. The right panels show the same, but with $J_z = 0.6$. For circulating trajectories, the minimum e and θ occur at $\omega = 0$. The dashed horizontal lines show the cosine of the critical Kozai inclination, $\sqrt{3/5}$. The separatrix—which separates circulating from librating trajectories—always has $e_0 = 0$ and $|\theta_{\pi/2}| = \sqrt{3/5}$.

and the evolution is typically similar to the SKM (except at extremely high inclinations). But as we shall show, if $\epsilon \gtrsim 0.01$, then the octupole term can lead to qualitatively new behavior that is not found in the $\epsilon = 0$ limit.

3. THE STANDARD KOZAI MECHANISM ($\epsilon = 0$)

We review the SKM to set the stage for the EKM. For the SKM, the planet’s orbit is circular ($\epsilon = 0$, i.e. $F = F_{\text{qu}}$). Hence there are two constants of the motion, F and J_z , and the motion is regular. Each trajectory may be labelled by the values of F and J_z . Inserting Equation (3) into Equation (10) immediately determines e as a function of ω , as well as θ as a function of ω . The three left panels of Figure 1 show sample trajectories, with fixed $J_z = 0.2$ and various values of F ; the right panels show the same, but with $J_z = 0.4$. For our purposes, the most important properties of the SKM are as follows:

- Because $J_z = \text{constant}$, each trajectory traces out a curve in the e - θ plane, which we call a “Kozai curve.”
- There are two classes of trajectories, librating and circulating. On circulating trajectories, e and $|\theta|$ are smallest at $\omega = 0$, and they are largest at $\omega = \pm\pi/2$. The separatrix has $e_0 \equiv e|_{\omega=0} = 0^5$ and $|\theta_{\pm\pi/2}| = \sqrt{3/5}$.

⁵ Throughout this paper, we denote values at $\omega = 0$ with subscript ‘0’.

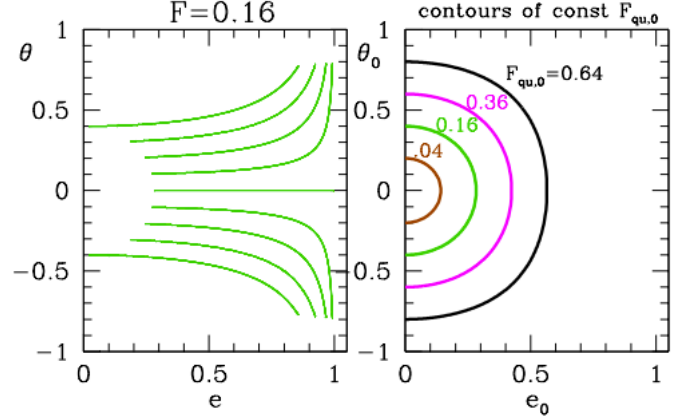


FIG. 2.— SKM ($\epsilon = 0$): The left panel shows trajectories with fixed F and various values of J_z (“Kozai curves”). The left-most tips of the Kozai curves (with co-ordinates $\{e_0, \theta_0\}$) trace out another curve, which we call the “energy curve.” That energy curve is shown in green in the right panel; it is the level curve of $F_{\text{qu},0} \equiv F_{\text{qu}}|_{\omega=0} = 0.16$. The right panel also shows some other energy curves. These intersect the θ_0 axis at $\sqrt{F_{\text{qu},0}}$ and the e_0 axis at $\sqrt{F_{\text{qu},0}/2}$.

- On a trajectory that has $e_0 \ll 1$, the largest e is

$$e_{\pm\pi/2}^2 \approx 1 - \frac{5}{3}\theta_0^2 \approx 1 - \frac{5}{3}J_z^2, \quad (12)$$

to leading order in e_0^2 , when $|\theta_0| < \sqrt{3/5}$. (The corresponding inclinations are the critical Kozai angles $\cos^{-1} \pm \sqrt{3/5} = 39^\circ$ and 141° .) Therefore when $|\theta_0| \ll 1$ (i.e. inclination close to 90°), the largest eccentricity is nearly unity.

- Given F and J_z , the minimal e on a circulating trajectory satisfies

$$e_0^2 = \frac{1}{2}(F - J_z^2). \quad (13)$$

Figure 2, left panel, shows a sequence of Kozai curves with the same F and differing J_z . The left boundaries of the sequence (i.e., the values $\{e_0, \theta_0\}$ for each Kozai curve) trace out a curve in the e - θ plane, which we call an “energy curve.” That curve is plotted in green in the right panel of Figure 2. An energy curve is a curve of constant $F_{\text{qu}}|_{\omega=0}$. Its form is given by Equation (13) with $J_z^2 = e_0^2(1 - \theta_0^2)$. The right panel of Figure 2 also shows other energy curves with different energies F_{qu} .

4. THE ECCENTRIC KOZAI MECHANISM ($\epsilon > 0$)

When the planet is eccentric ($\epsilon > 0$) there is only a single conserved quantity, the secular energy F . Therefore the particle’s trajectories are more complicated, and can even be chaotic. Figure 3 shows two sample trajectories in the e - θ plane for $\epsilon = 0.01$. Both trajectories have the same energy $F = 0.16$, but different initial conditions consistent with that energy. Rather than being confined to a single Kozai curve, the particle evolves from one Kozai curve to another. As long as $\epsilon \ll 1$, all of these Kozai curves have nearly the same F_{qu} , and therefore the trajectories in Figure 3 follow along the tracks displayed in the left panel of Figure 2.

Trajectory ‘a’ in Figure 3 evolves through $\theta = 0$. Its orbit flips from prograde ($\theta > 0$) to retrograde ($\theta < 0$)

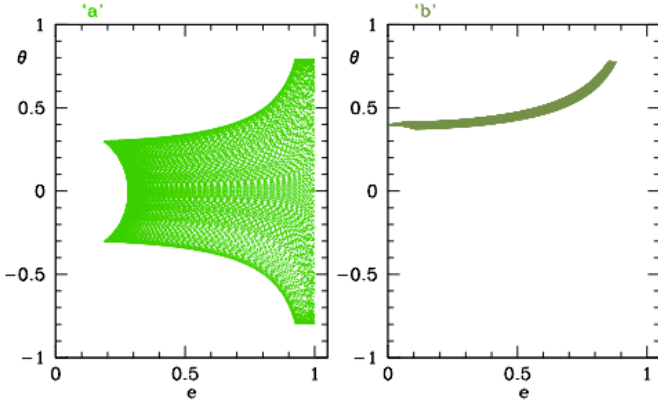


FIG. 3.— EKM: Two sample trajectories ('a' and 'b') with $F = 0.16$, $\epsilon = 0.01$, and different initial conditions. When the planet is eccentric, the test particle no longer traces out a single Kozai curve, but evolves from one Kozai curve to another, approximately tracing out a sequence of Kozai curves that have a fixed quadrupole energy (Fig. 2, left panel). Orbit 'a' flips repeatedly (i.e. crosses $\theta = 0$) and reaches extreme eccentricities, and orbit 'b' does not. Although only points up to time $t = 500$ are plotted, longer runs yield identical plots, albeit with more densely packed points. In particular, orbit 'b' never flips.

and back again. Furthermore, its eccentricity approaches unity. In fact, the flipping of an orbit is closely tied to its eccentricity reaching unity. This can be seen from Equation (12), which implies that a Kozai curve that has $\theta_0 \approx 0$ reaches $e \approx 1$. (It never reaches exactly $e = 1$; see below). Trajectory 'b' never flips, and its eccentricity does not approach unity.

The left panels of Figure 4 show the temporal evolution of θ and e for trajectory 'a'. The bottom left panel shows two angles that appear as arguments of cosine terms in F_{oc} . When the particle's orbit is prograde, the angle $\omega + \Omega$ librates and $\omega - \Omega$ circulates; and when it is retrograde, those two angles switch roles. The right panels of Figure 4 show the same quantities for trajectory 'b'. Whereas trajectory 'a' is regular, 'b' is chaotic. We demonstrate that more explicitly below.

The left panels of Figure 5 are a zoom-in of the 'a' trajectory at early times. The fast oscillations in θ and e are primarily governed by the quadrupole evolution, as e and θ trace out Kozai curves with $F = 0.16$ and various values of J_z . Over the course of a single oscillation, ω increases from 0 to π or from $-\pi$ to 0. Hence the orbit is always circulating (see Fig. 1). The top left panel also shows J_z . Whereas in the SKM $J_z = \text{const.}$, here J_z changes in a nearly step-wise fashion. There are sharp jumps in J_z whenever e and θ change rapidly; these are forced by the octupolar contribution F_{oc} . The long-term evolution of J_z controls the envelopes of both θ (Fig. 5, top-left panel) and e (Fig. 5, middle-left panel; see eq. [12]). Successive maxima of e occur in discrete steps. Therefore even when J_z crosses through zero, the maximum e is never precisely unity. Nonetheless, as time evolves, the maximum e reached approaches closer and closer to unity.

The right panels of Figure 5 show the corresponding zoom-in for trajectory 'b'. The bottom right panel shows that ω switches from circulation to libration and back again. That explains why the 'b' trajectory is chaotic. Similar behavior is shown in Holman et al. (1997).

A global view of the dynamics is provided by surfaces of

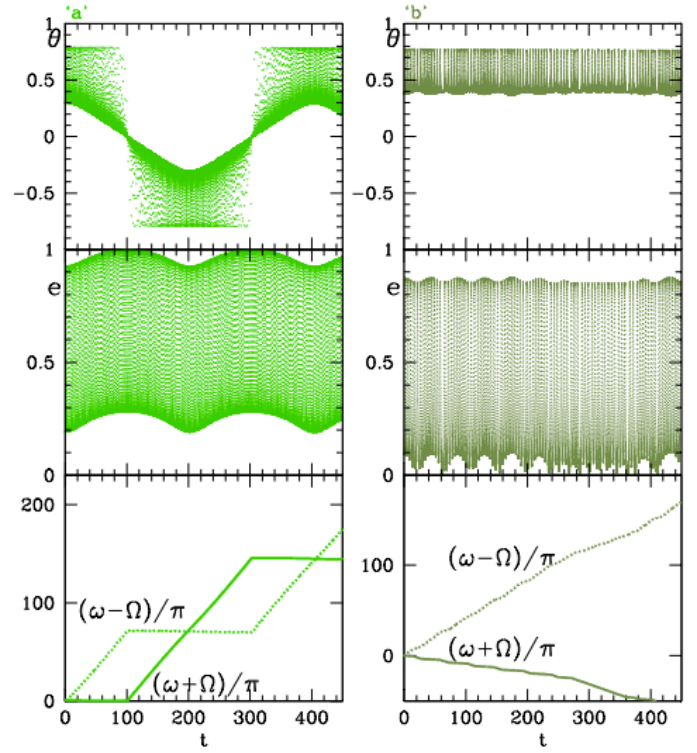


FIG. 4.— EKM: Temporal evolution of the two trajectories depicted in Figure 3. In the bottom panels, the angles are cumulative. Trajectory 'a' reaches extreme eccentricities when it flips. Its evolution is regular, with $\omega + \Omega$ librating when it is prograde, and $\omega - \Omega$ librating when it is retrograde. Trajectory 'b' is chaotic, and never flips.

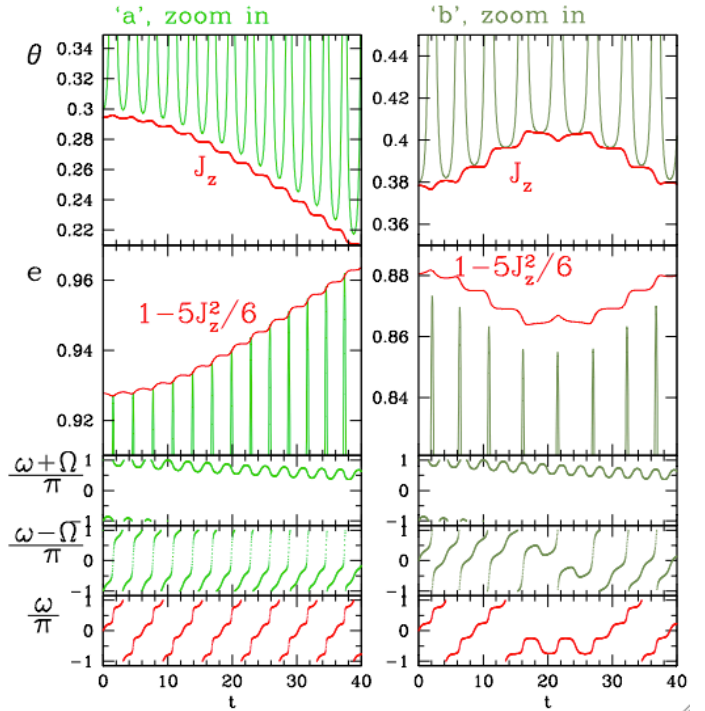


FIG. 5.— EKM: Zoomed in evolution of trajectories 'a' and 'b' at early times (Fig. 3). In the top panels the red lines show that J_z controls the envelope of both θ and e (via eq. [12]). In the bottom panels, the angles are not cumulative.

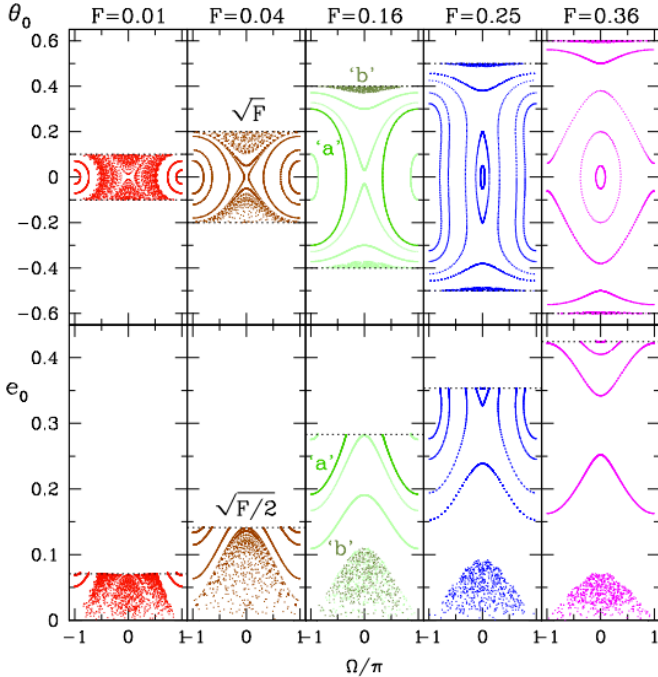


FIG. 6.— EKM, $\epsilon = 0.01$. Surfaces of section with various values of F ; points are plotted whenever $\omega = 2n\pi$ for integer n . For each F , if the values of θ_0 were plotted against the value of e_0 , they would lie along an energy curve (Fig. 2, right panel). The colors in that figure correspond to the colors in this one.

section. Figure 6 maps out the behavior when $\epsilon = 0.01$. We plot a point whenever $\omega = 2n\pi$ for integer n .⁶ This may be interpreted as follows. Consider trajectory ‘a’ of Figure 3. When $\omega = 2n\pi$ that trajectory hits the green energy curve depicted in the right panel of Figure 2. At those times we plot in Figure 6 the value of $e = e_0$ versus Ω and $\theta = \theta_0$ versus Ω (curves labelled ‘a’, middle panels). Also shown in those green middle panels are other trajectories with the same energy $F = 0.16$, including trajectory ‘b’. If all of the green points were plotted against each other in the e_0 - θ_0 plane, they would trace out the energy curve labelled 0.16 in Figure 2. Equivalently, one can imagine that that energy curve is extended out of the plane of the paper into a half-cylinder, with the third dimension being the value of Ω . The $F = 0.16$ surfaces of section of Figure 6 cover the surface of that half-cylinder. Of course, for a given energy, the maximum $|\theta_0|$ is \sqrt{F} , and the maximum e_0 is $\sqrt{F/2}$. Beyond those values, the energy curve does not exist (Fig. 2 caption).

The other panels in Figure 6 may be interpreted similarly, with each pair of panels at fixed F lying along a single energy curve of Figure 2 (with corresponding colors). We therefore now have a virtually complete view of the $\epsilon = 0.01$ dynamics.

Perhaps the most dramatic new behavior caused by the octupole term is that orbits can flip orientation (i.e. cross $\theta = 0$), and, as a consequence, reach arbitrarily high values of eccentricity. From Figure 6, it is immediately clear which orbits exhibit this behavior, and which do not, at $\epsilon = 0.01$. For example, orbits with $e_0 = 0$ will

⁶ Trajectories only appear on our sections while ω is circulating, because ω is never equal to $2n\pi$ during librations (Fig. 1).

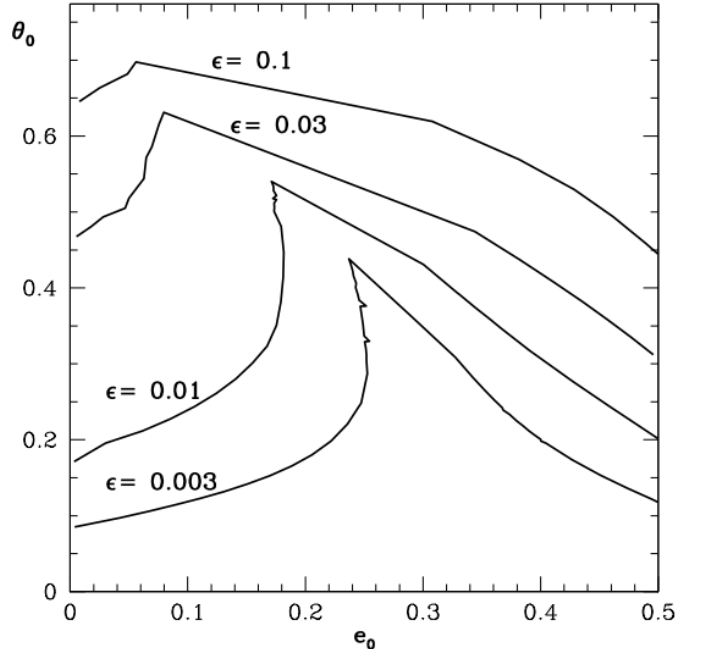


FIG. 7.— First Flipping Orbit. Each curve marks the first flipping orbit that can occur for a given value of ϵ . Above each curve (i.e., at low inclination) none of the orbits flip, and below it some do.

always flip provided that $|\theta_0| \lesssim 0.2$ (i.e., $i_0 \gtrsim \cos^{-1} 0.2 \sim 80^\circ$ for prograde orbits). For $e_0 \neq 0$, we infer from the blue ($F = 0.25$) panels that even orbits with θ_0 as large as 0.4 (i_0 as small as 66°) can flip.

A second new behavior is the appearance of chaos. Regular orbits appear as curves in the surfaces of section, while chaotic orbits appear as a smattering of points. For example, it is apparent from Figure 6 that trajectory ‘a’ is regular and ‘b’ is chaotic. Chaos always occurs near $e_0 = 0$. That is because the Kozai separatrix always has $e_0 = 0$ (Section 3), and chaos is caused the crossing of the Kozai separatrix, when ω transitions from librating to circulating and back to librating (e.g., Fig. 5).

Figure 7 is the main result of this paper. It summarizes where flipping orbits occur for various values of ϵ . Towards the top of the plot (large θ_0 and small i_0), there are no flipping orbits. But as θ_0 decreases, an increasing number of orbits can flip. Each curve marks, for a given ϵ , the location at which the first flipping orbit occurs, if Ω is judiciously chosen. Above the curve there are no flipping orbits, and below there are some—typically around half of the orbits below the curve can flip. We made this plot by running a suite of numerical simulations initialized with $\theta = 0$ and $\omega = 0$, and scanning through values of initial e and Ω to determine which flipping orbit reached the largest values of θ_0 for a given initial e , and then plotting the extreme values of e_0 and θ_0 for that orbit. (Note that all such trajectories initialized with the same initial $e = e_0$ share the same energy curve.)

A striking feature of Figure 7 is the fairly sudden transition when ϵ exceeds a few percent. For example, focusing on orbits with $e_0 = 0$, when $\epsilon = 0.01$ flipping orbits can occur only if $|\theta_0| \lesssim 0.2$ i.e., $i_0 \gtrsim 80^\circ$ (for prograde), as stated above. But for $\epsilon = 0.03$ flips can occur for $|\theta_0| \sim 0.5$, i.e. $i_0 \sim 60^\circ$ (for prograde). Note that if test particle orbits are randomly oriented, they will be uni-

formly distributed in θ , and therefore half of the orbits will have $\theta < 0.5$. Of course, this is only a rough estimate for the fraction of flipping orbits, since it depends also on the values of the other variables (e, ω, Ω).

The curves in Figure 7 rise as e_0 increases from 0, and then suddenly turn over. The reason for the sudden turn over is apparent from a glance at the surfaces of section (Fig. 6). In the blue ($F = 0.25$) section, there are flipping orbits centered both on $\Omega = 0$ and on $\Omega = \pi$, with the latter ones reaching to a larger $|\theta_0|$. But in the magenta ($F = 0.36$) section, there are no more flipping orbits centered at $\Omega = \pi$. It is that discontinuity that gives rise to the sharp break in Figure 7.

5. SUMMARY

In this paper, we map out the behavior of a test particle that is forced by a massive eccentric planet, working under the secular octupole approximation.

In Section 2, we give the evolutionary equations. These are derived in the Appendix, where we show how one may use the published Hamiltonian—which has had its nodes eliminated—to derive the full equations of motion. There is a single parameter, ϵ , that characterizes deviations from the SKM (Eq. [9]). The SKM is recovered when $\epsilon \ll 1$, i.e. when the planet is either nearly circular or very distant.

In Section 3, we review the SKM. In the e - θ plane (where $\theta \equiv \cos i$), the particle traces out a Kozai curve because its J_z is fixed. A sequence of Kozai curves with the same energy F outline an energy curve, which is a curve of constant secular energy, evaluated at $\omega = 0$.

In Section 4, we map out what happens when the planet’s orbit is eccentric. Our principal results are:

- In the e - θ plane, a single trajectory evolves from one Kozai curve to another, all of which about the same energy curve (Fig. 3).
- For trajectories where the orbit flips, the eccentricity becomes extremely high, and as time evolves, the maximum eccentricity reached approaches closer and closer to unity. That is because every time θ crosses through zero, $|\theta_0|$ becomes very small. And given enough zero-crossings, the smallest $|\theta_0|$ reached becomes arbitrarily small, and hence the maximum eccentricity becomes arbitrarily close to unity (as determined by Eq. [12]).
- The vertical angular momentum J_z varies gradually in the EKM, unlike in the SKM where it is constant. Its evolution controls that of both θ and e (Fig. 4). Even when the value of ϵ is small, and hence the temporal evolution of J_z is slow, if J_z crosses through zero, the dramatic flipping and extreme eccentricity behavior occurs (Fig. 3, left panel).
- Chaotic behavior occurs when the Kozai separatrix is crossed. In that case, ω transitions from librating

to circulating, and back. See also Holman et al. (1997).

- Surfaces of section, taken whenever $\omega = 2n\pi$, provide an graphical global map of the dynamics. Each energy curve gives rise to two panels in Figure 6 (top and bottom). By stepping through the energy curves, one acquires a complete map of the dynamics for a given value of ϵ . From the surfaces of section, one can immediately see which orbits exhibit flipping and extreme eccentricity, and which do not. One can also see which orbits are chaotic and which are not. All four combinations occur: flipping and non-chaotic (‘a’), flipping and chaotic, non-flipping and non-chaotic, non-flipping and chaotic (‘b’).
- Figure 7 is the main result of this paper. For each ϵ , it gives the curve in the e_0 - θ_0 plane at which the first flipping orbit occurs (along with the accompanying extreme-eccentricity behavior). Above the curve no flipping orbits occur, and below it an increasing number occur. There is a fairly sharp transition in the smallest inclination at which orbits can flip. For $\epsilon \sim 0.01$, the inclination must exceed $\sim 80^\circ$ to flip (for prograde orbits with $e_0 = 0$); but when $\epsilon \sim 0.03$, it need only exceed $\sim 60^\circ$, implying that around half of randomly oriented test particle orbits will flip in that case.

We have made a number of approximations in order to simplify the analysis. First, we work under the secular octupole approximation, which is poor when ϵ is too large because in that case the particle comes close to the planet. We have made a few comparisons with direct integrations, some of which are presented in Naoz et al. (2011b). Thus far the agreement is quite good, but more should be done to determine the domain of validity of the secular octupole approximation. Second, we take the inner orbiting body to be massless. While that is appropriate for a planet being forced by a companion star, it is not for two planets, which is the main motivation for this paper (Naoz et al. 2011a). We are currently extending the work presented here to two massive planets; in that case, there is a generalized ϵ that includes the masses (Naoz et al. 2011b). And third, we ignore all physical effects beyond Newtonian gravity, including tides and general relativistic precession. These will play a role when the inner planet’s eccentricity approaches unity.

ACKNOWLEDGMENTS

We thank W. Farr, B. Katz, F. Rasio, J. Teyssandier, and Y. Wu for helpful discussions. SN acknowledges support from the Gruber Foundation Fellowship and from the National Postdoctoral Award Program for Advancing Women in Science (Weizmann Institute of Science).

REFERENCES

- Blaes, O., Lee, M. H., & Socrates, A. 2002, *ApJ*, 578, 775
 Eggleton, P. P. & Kiseleva-Eggleton, L. 2001, *ApJ*, 562, 1012
 Fabrycky, D. & Tremaine, S. 2007, *ApJ*, 669, 1298
 Ford, E. B., Kozinsky, B., & Rasio, F. A. 2000, *ApJ*, 535, 385
 —. 2004, *ApJ*, 605, 966

Harrington, R. S. 1968, PhD thesis, THE UNIVERSITY OF TEXAS AT AUSTIN.
 —. 1969, *Celestial Mechanics*, 1, 200
 Holman, M., Touma, J., & Tremaine, S. 1997, *Nature*, 386, 254
 Kozai, Y. 1962, *AJ*, 67, 591
 Krymolowski, Y. & Mazeh, T. 1999, *MNRAS*, 304, 720
 Laskar, J. & Boué, G. 2010, *A&A*, 522, A60+
 Lidov, M. L. & Ziglin, S. L. 1976, *Celestial Mechanics*, 13, 471
 Marchal, C. 1990, *The three-body problem*, ed. Marchal, C.
 Murray, C. D. & Dermott, S. F. 2000, *Solar System Dynamics* (Cambridge University Press)
 Naoz, S., Farr, W. M., Lithwick, Y., Rasio, F. A., & Teyssandier, J. 2011a, *Nature*, 473, 187

—. 2011b, submitted
 Thompson, T. A. 2010, ArXiv e-prints
 Triaud, A. H. M. J., Collier Cameron, A., Queloz, D., Anderson, D. R., Gillon, M., Hebb, L., Hellier, C., Loeillet, B., Maxted, P. F. L., Mayor, M., Pepe, F., Pollacco, D., Ségransan, D., Smalley, B., Udry, S., West, R. G., & Wheatley, P. J. 2010, *A&A*, 524, A25+
 Wu, Y. & Murray, N. 2003, *ApJ*, 589, 605

APPENDIX

OCTUPOLE SECULAR EQUATIONS OF MOTION FOR A TEST PARTICLE

The secular interaction energy between an interior and exterior planet (unprimed and primed, respectively) can be written as

$$E_{\text{eon}} = -G_N \frac{mm'}{a'} \alpha^2 f(\alpha, e', e, g', g, \theta), \quad (\text{A1})$$

where $\theta \equiv \cos I$ and the other quantities are the mutual inclination I , argument of periaapse g , eccentricity e , semimajor axis a , ratio of semimajor axes (inner to outer) α , mass m , and Newton’s constant G_N . (The notation here differs slightly from the body of the paper in order to connect to previous treatments of the octupole. See footnote 3 for the relation between the two notations.) The subscript “eon” refers to the elimination of the nodes, i.e. the longitudes of ascending nodes (h, h') have been chosen to satisfy $h - h' = \pi$ which is why they do not appear in the energy.

We seek the equations of motion for the inner planet in the limit that $m \rightarrow 0$. The equations of motion can be expressed as Hamilton’s equations for the canonical Delaunay variables $\{g, G; h, H\}$ where

$$G \equiv m\sqrt{G_N M_* a} \sqrt{1 - e^2}, \quad H \equiv G \cos i, \quad (\text{A2})$$

with M_* the mass of the central star. Note that in secular theory, a is constant; note also that in the test particle limit, $i = I$.

Setting the Hamiltonian $\mathcal{H} = E_{\text{eon}}$ will give the correct equations of motion of g, G , and h , but not for H because the nodes have been eliminated (Naoz et al. 2011b). We shall prove that the correct procedure for obtaining the Hamiltonian is simply to replace $g' \rightarrow \pi - h$ in the above expression for E_{eon} , as well as $e' = \text{const.}$, $e^2 \rightarrow 1 - G^2/(m^2 G_N M_\odot a)$, and $\theta \rightarrow H/G$. The relation $g' \rightarrow \pi - h$ might appear surprising because one might have expected that $g' = \text{const}$ when the inner particle is massless. But in truth h' is undefined because the reference plane is aligned with the outer orbit. Therefore, the outer planet must only have $g' + h' = \text{const.}$, and we may choose without loss of generality the constant to equal zero. Hence, elimination of the nodes implies $g' = \pi - h$.

Proof

Our proof is based on the triangle equality $G^2 + G'^2 + 2GG'\theta = (H + H')^2$, which expresses the square of the vertical angular momentum in two equivalent ways. Taking the time derivative of the triangle equality, and noting that both G and G' satisfy Hamilton’s equations, i.e. $dG/dt = -\partial E_{\text{eon}}/\partial g$ and $dG'/dt = -\partial E_{\text{eon}}/\partial g'$, we find that to leading order in m , $dG'/dt = -\frac{d}{dt} G\theta$, i.e. $dH/dt = \partial E_{\text{eon}}/\partial g'$ which proves that if we replace $g' \rightarrow \pi - h$ in E_{eon} , we will end up with the correct Hamilton equation for H .

Equations of Motion

We may re-scale all momenta by an arbitrary constant without changing the equations of motion as long as we rescale the Hamiltonian by the same constant. Therefore defining

$$J \equiv \frac{G}{m\sqrt{G_N M_* a}} \equiv \sqrt{1 - e^2} \quad (\text{A3})$$

$$J_z \equiv J \cos I \equiv \theta \sqrt{1 - e^2}, \quad (\text{A4})$$

the rescaled Hamiltonian is

$$\mathcal{H}(J, g; J_z, h) \equiv \frac{E_{\text{eon}}}{m\sqrt{G_N M_* a}} \quad (\text{A5})$$

$$= -\frac{m'}{M_*} \Omega_* \alpha^3 f(\alpha, e', e, g', g, \theta), \quad (\text{A6})$$

where Ω_* is the orbital angular speed of the test particle around the star.

The expression for f (defined via eq. [A1]) is derived, e.g., in Ford et al. (2000) to octupole order. We re-express their Equation (22) in the limit $m, m' \ll M_*$ as

$$f = \frac{3}{8} \frac{1}{(1 - e'^2)^{3/2}} (F_{\text{qu}} + \frac{\alpha e'}{1 - e'^2} F_{\text{oc}}) , \quad (\text{A7})$$

where F_{qu} and F_{oc} are displayed above (Eqs. 10 and 11, with $g \equiv \omega$ and $h \equiv \Omega$) after correcting the sign of the octupole term (Ford et al. 2004) and replacing $g' \rightarrow \pi - h$

The equations of motion are Hamilton's equations for Hamiltonian (A6). These are displayed explicitly in the body of the paper (Eqs. [4]-[7]) after defining the rescaled time

$$t \equiv T \times \frac{m'}{M_*} \Omega_* \alpha^3 \frac{3}{8} \frac{1}{(1 - e'^2)^{3/2}} , \quad (\text{A8})$$

where T is the true time.